Evaluation of the IGRF-13 Main Field 2020, and Predictive Secular Variation 2020 – 2025

Ropp Guillaume[1], Baerenzung Julien[2], Lesur Vincent[1], and Holschneider Matthias[2]

[1] Université de Paris, Institut de physique du globe de Paris, CNRS, F-75005 Paris, France.
[2]Institute for Mathematics, University of Potsdam

November 22, 2019

1 Introduction

In this short note we evaluate two components of the IGRF-13, the Main field 2020 and the predictive SV 2020 – 2025. The results are presented in the two next sections.

We follow here the same coding suggested by Patrick Alken for the institution team. It is reported in Table (1).

2 Main Field 2020 evaluation

Twelve candidate models have been submitted for building the IGRF-13 main field 2020. Reading through the model descriptions we note that one candidate – the candidate **B** – is based on a completely independent data set, whereas all other candidates rely on the Swarm satellite mission data set. Some candidates – e.g. candidate **O** – rely significantly on observatory data. The techniques used for modelling differ significantly from one candidate to the next, particularly regarding the way the geomagnetic field time variations have been handled. We point out that the candidate **C** process their data for external field perturbations using the output of a model very similar to the candidate **D** . These two models are therefore not fully independent.

To estimate the quality of the candidates to the IGRF-13 main field for epoch 2020, we proceed in two ways. First we made cross-comparisons between the candidate models, and secondly, we compared the field model values with the most recent definitive (or quasi-definitive) data series of few IPGP observatories. Results obtained for these two approaches are described in the two following sub-sections 2.1, 2.2.

2.1 cross-comparison

The cross-comparisons of the model candidates are made relative to their mean and median models, the latter being probably a better reference than the former. We use the global measure of the differences given in equation (1), where

Table 1: Coding for for the institution team

A	BGS candidates
B	CEA_CSES candidates
C	CU_NCEI candidates
D	DTU candidates
E	GFZ candidates
F	IPGP candidates
G	ISTerre candidates
H	IZMIRAN candidates
I	Japanese Team candidates
J	Leeds candidates
K	Max Plank candidates
L	NASA_GSFC candidates
M	Potsdam_MaxPlank candidates
N	Spanish Team candidates
O	Strasbourg candidates

Table 2: *rms* differences, as estimated through equation (1), of the candidate models relative to the median and mean of the candidates. Maximum absolute difference between the vertical down component of the candidate models and the median model, calculated on a 1 degree grid on a sphere of radius $a = 6371.2$km.

	A	**B**	**C**	**D**	**E**	**F**	**G**	**H**	**L**	**M**	**N**	**O**
rms median	5.09	11.14	6.56	2.48	15.96	4.18	8.93	6.66	7.62	3.40	8.93	12.84
rms mean	4.61	10.56	7.12	3.69	14.88	4.93	8.93	7.69	6.42	4.74	8.62	12.14
max |differ.|	13.0	23.7	19.5	7.1	54.1	15.5	21.8	17.9	14.9	10.0	74.6	30.8

the reference model Gauss coefficients (– i.e. the mean and median model Gauss coefficients) are the $\bar{g}_l^m$.

$$rms = \sqrt{\sum_{\{\ell,m\}} (\ell+1)(\bar{g}_l^m - g_l^m)^2} \tag{1}$$

We point that such a measure tends to give a significant weight to the small scale components of the models. The obtained results are synthesised in table (2). We identify three models with particularly large *rms* values: the **B** , **E** and **O** models. The **G** and **N** models differ also significantly from the reference models.
To explore further the differences between candidate models, we look at differences for each Gauss coefficient. The results are presented in Figure 1. Large differences are seen for g_1^0. This is expected, and probably not a major problem, because the induced fields are large for this component, and the obtained g_1^0 value depends on the way these induced fields are handled. Candidates **L** and **O** present the largest differences for this Gauss coefficient. More worrying are the large differences for other Gauss coefficients and here again we identify the candidates **E** , **B** , **G** and, to a lesser extent **O** . For the latter, we notice relatively high differences at high spherical harmonic degrees certainly due to the fact that the model is based mainly on observatory data.

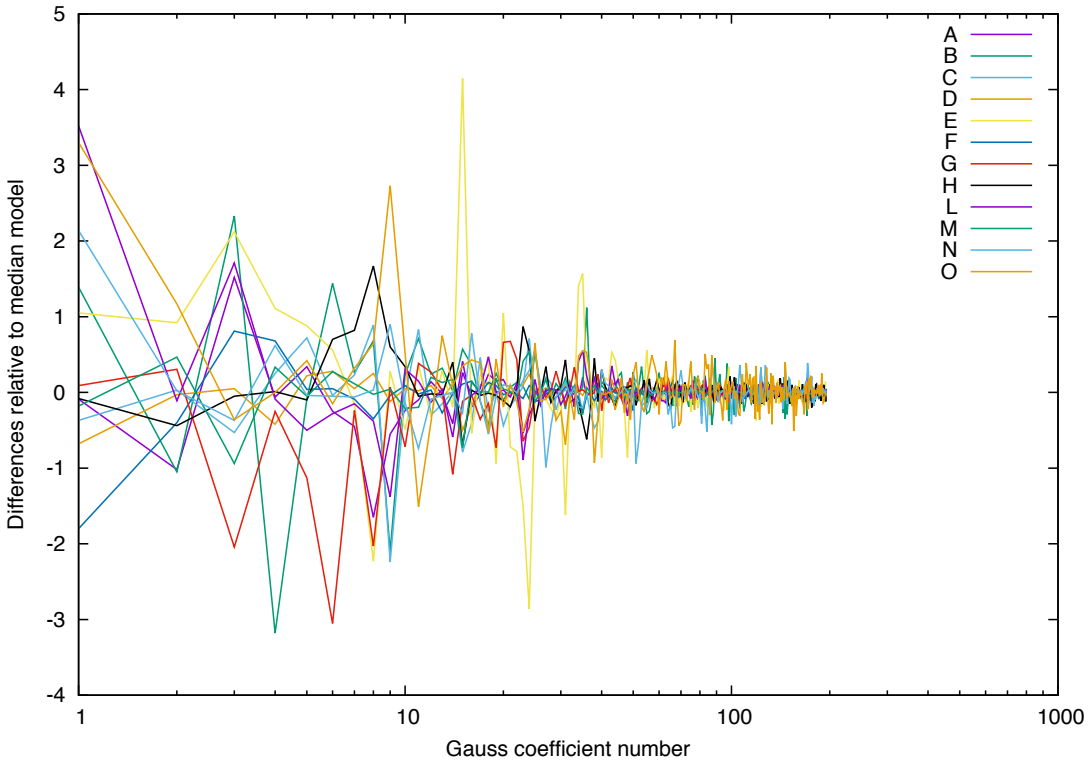

Figure 1: Differences between Gauss coefficient candidates and those of the median model. The Gauss coefficients are set in canonical order(– i.e. $g_1^0, g_1^1, h_1^1, g_2^0, g_2^1, \cdots$).

Finally we looked at the differences relative to the median model when the candidates are mapped on a sphere at Earth's reference radius. The absolute maximum differences are given in Table 2, but this provides only a partial view of the differences between models. It is more informative too look at the maps in Figure (2). Some candidate models present significant differences but these are close to the poles (– e.g. candidate **N**), the models being otherwise similar to the median model. Other candidates have large spread of large differences, mainly models **B** , **E** and **O** .

2.2 Comparison with observatory data

For a further evaluation of the candidate models, we compared them with time series of the observed magnetic field at four observatories: CLF, BOX, TAM and KOU. We used daily means of vector observations that have been rotated in

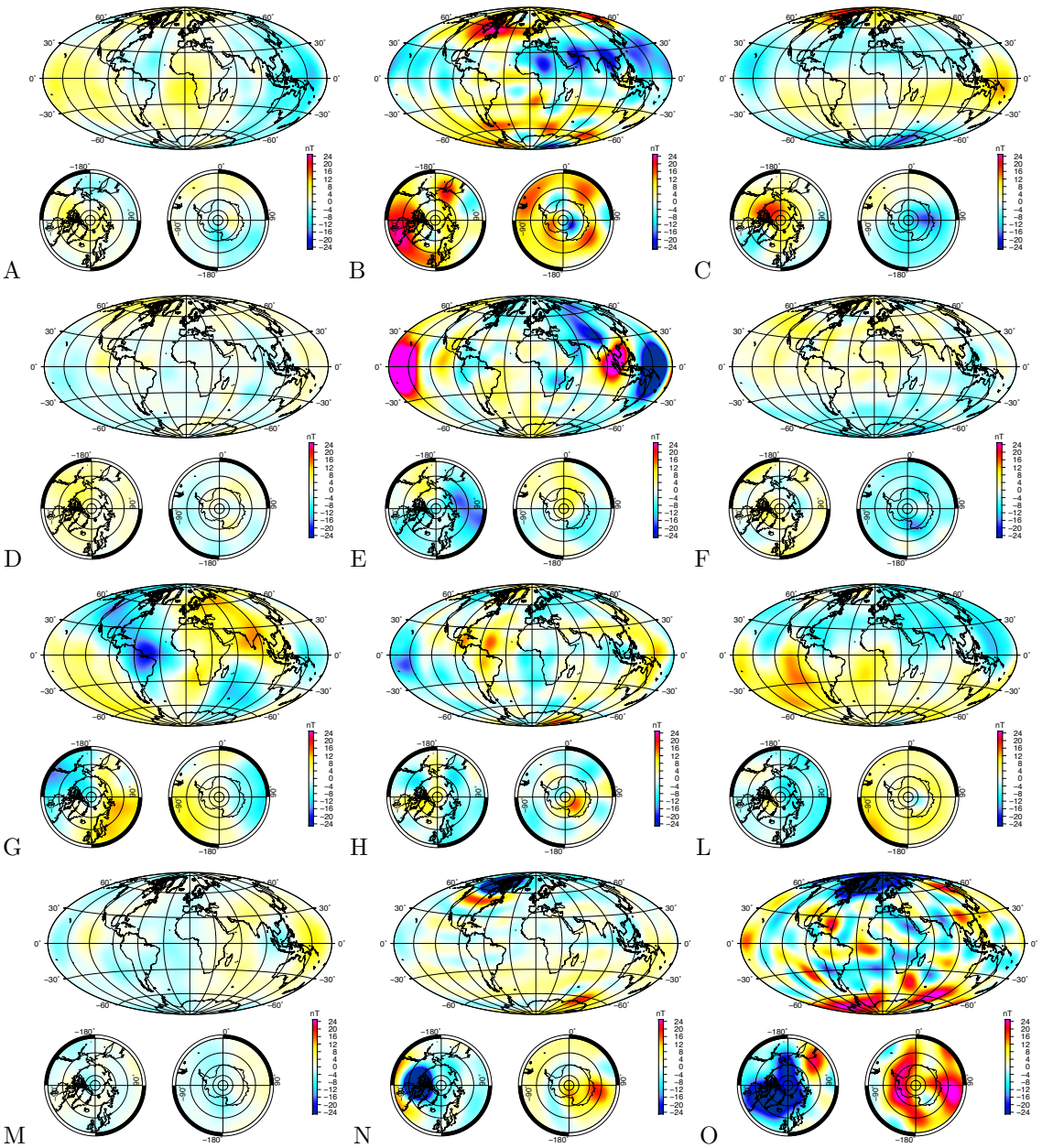

Figure 2: Maps of vertical down differences between candidate models and median model at the Earth's reference radius $a = 6371.2$km. Colours saturate outside the ± 25nT interval

geocentric North, East and Down directions. The data used are quasi-definitive data for 2019, and definitive data for previous years. The data set includes the data from October 2019. Direct comparisons of models and observatory time series are usually difficult because of the lithospheric field contributions. These can be large for observatories but are nearly negligible in candidate field models. We circumvent this difficulty by adjusting the observatory data such that the monthly mean values observed in 2015.0 match the DGRF-2015 candidate median. The adjusted observatory time series remain however contaminated by external fields, so the comparisons with models should be interpreted with some caution.

We identified in Figure (3) three anomalous model values: one in the CLF North component, one in KOU East component and one in the TAM vertical down component. These correspond to the models **B** and **O** respectively. There is another possible anomalous value in the TAM vertical down component, corresponding to model **C** , but this is questionable given the approximations of the method we used here.

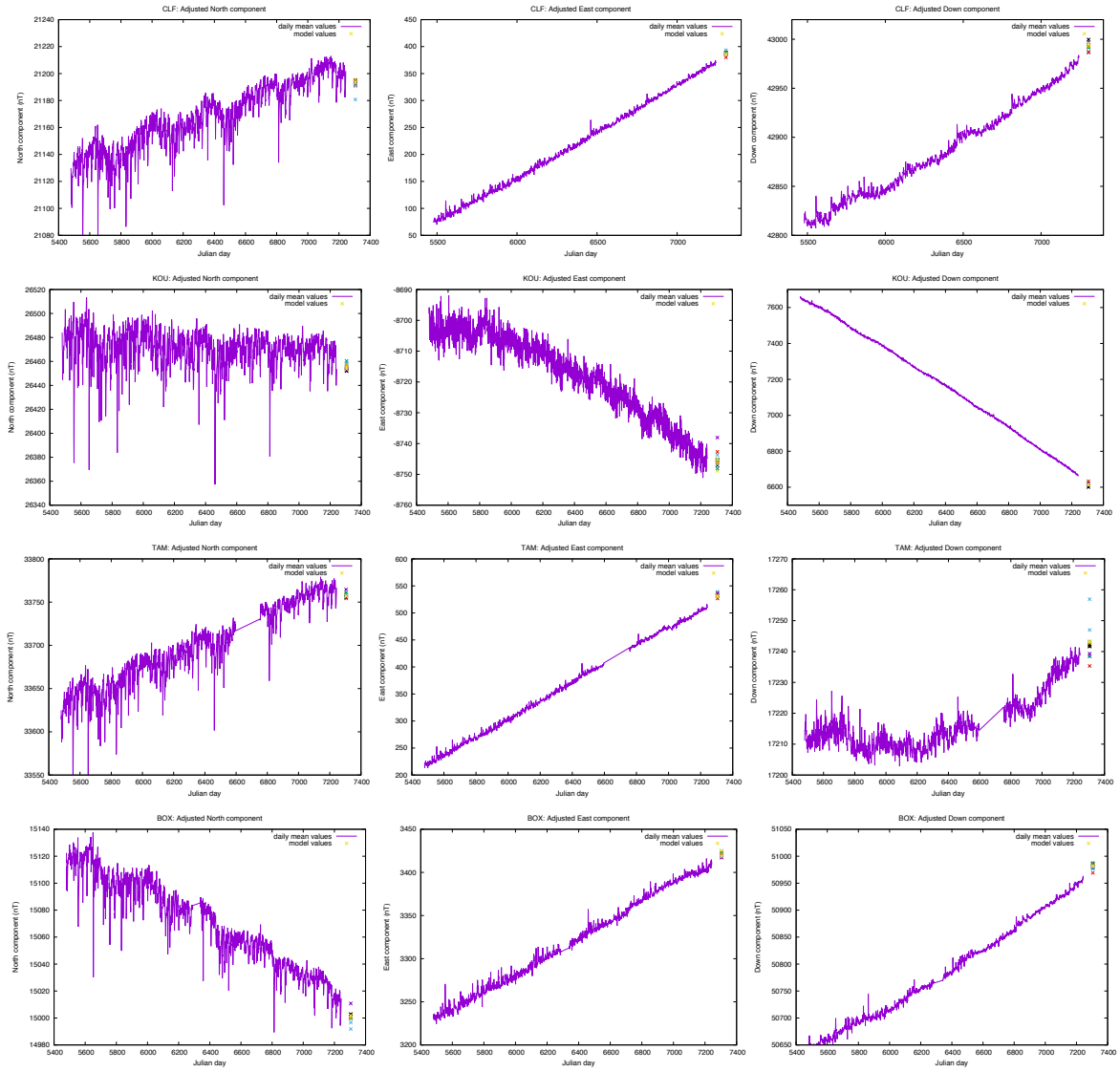

Figure 3: Comparison of the adjusted daily mean data of four observatories with the estimated main field IGRF candidate values. From top to bottom: CLF, KOU, TAM and BOX observatories. From left to right: North, East and Down components.

3 Secular Variation 2020 – 2025 evaluation

The proposed candidates for the secular variation prediction over five years (2020 – 2025) are evaluated through their correspondence with the 'Kalmag' model of the University of Potsdam. The predictions from the Kalmag model are controlled using a time series from the Chaos-6 model of Finaly2016.
All of the 14 candidates submitted for the IGRF-13 are evaluated.
The evaluation of the different predictions is performed :

- At the location of 10 ground based observatories
- On the total surface of the Earth

- For several individual (large scale) spherical harmonics coefficients

3.1 Observatories time series

The secular variation of the different candidate models is evaluated at several ground based observatory locations and is displayed on figures 4 and 5. The color assignment for each model is given on the top of both figures. The figures are organised as follows: from top to bottom the geographic latitude of the various ground based observatories (shown on the left together with the IAGA observatory code) is decreasing, and from left to right, the radial, azimuthal and longitudinal components of the secular variation are respectively shown. Together with the candidate models, time series between 2000.0 and 2025.0 of the secular variation deriving from the CHAOS-6 model (black lines), monthly mean of observatory measurements (blue dots) and the Kalmag model (red areas and red dashed lines) are also shown on the different panels. Note that the Kalmag solution presented with red area consists in the mean secular variation model plus and minus 2 standard deviation (σ), whereas the red dashed lines are associated with 5 years forecasts of the mean model $\pm 2\sigma$.
Most of the candidates predict a close behaviour for the $2020 - 2025$ secular variation. Nevertheless, three of them in particular differ at certain locations quite strongly from the mean solution, the **I**, the **L** and the **O** models. For the **O** model (dark blue lines), deviations from the mean predicted secular variation mostly occurs for its radial and azimuthal components, and the model is sometimes far beyond the 95% confidence interval predicted by the Kalmag estimation, as in MBour(MBO) or Learmonth(LRM). The **L** model (purple lines) clearly proposes the secular variation which differs the most from the other ones with discrepancies occurring independently of its components. As for the **O** model, the **L** model lies sometimes beyond our $\pm 2\sigma$ boundary as in Qaanaaq(THL), Niemegk(NGK) or Kakioka(KAK). Finally the **I** model (olive lines) is the last estimation exhibiting noticeable deviations from the other ones. Although less pronounced than for the **L** and **O** models theses deviations are clearly visible in a few locations like MBour or Mawson(MAW).
To globally evaluate the level of deviation of the three questionable models (**I** ,**L** ,**O**) with respect to the Kalmag model of Potsdam, we measured the portion of the Earth's surface where each component of these models (radial, azimuthal, longitudinal) were lying within the 95% confidence interval we predicted for 2022.5. The results in terms of percentage at the Earth's surface are summarised in table 3. Note that we tested the forecasting ability of our method by comparing 2.5 year predictions from 2005, 2010, and 2015 with the secular variation deriving from the CHAOS-6 model in 2007.5, 2012.5, and 2017.5. We noticed that our model was always overestimating the level of uncertainties associated with our mean predicted solution, providing therefore a pessimistic range of uncertainties.
Table 3 confirms that the model the less likely to be accurate with respect to the Kalmag prediction is the **L** model with only 75.8% to 82.1% of its secular variation estimates falling within our 95% confidence interval at the Earth's surface. It is followed by the **O** and **L** candidates in terms of compatibility with our forecast. However, the **O** secular variation only seems to have an issue with its dipolar component as it can also be observed on the top left panel of figure 6. The comparison between our forecast and the **O** secular variation with and without dipole clearly shows that the discrepancies between the two models come from the **O** dipolar component. Indeed, once removed, the proportion of the Earth's surface where the Kalmag and the **O** secular variations are compatible jump from 86.0% and 81.9% for respectively the radial and azimuthal components to 98% for both components. For the model **I** the situation is more mitigated since its range of agreement with the Kalmag prediction varies from 92.5% to 94.0% at the Earth's surface, which remains really close to the ideal case of 95%. Although the uncertainties of the Kalmag model are overestimated, one cannot clearly state that the **I** deviations are too large to discard the model.

Table 3: Portion of the secular variation at the Earth's surface lying withing the Kalmag 95% confidence interval in 2022.5

Model	$\partial_t B_r$	$\partial_t B_\theta$	$\partial_t B_\phi$
I	92.5%	94.2%	94.0%
L	75.8%	72.5%	82.1%
O	86.0%	81.9%	97.1%
O without dipole	98.0%	98.0%	97.1%

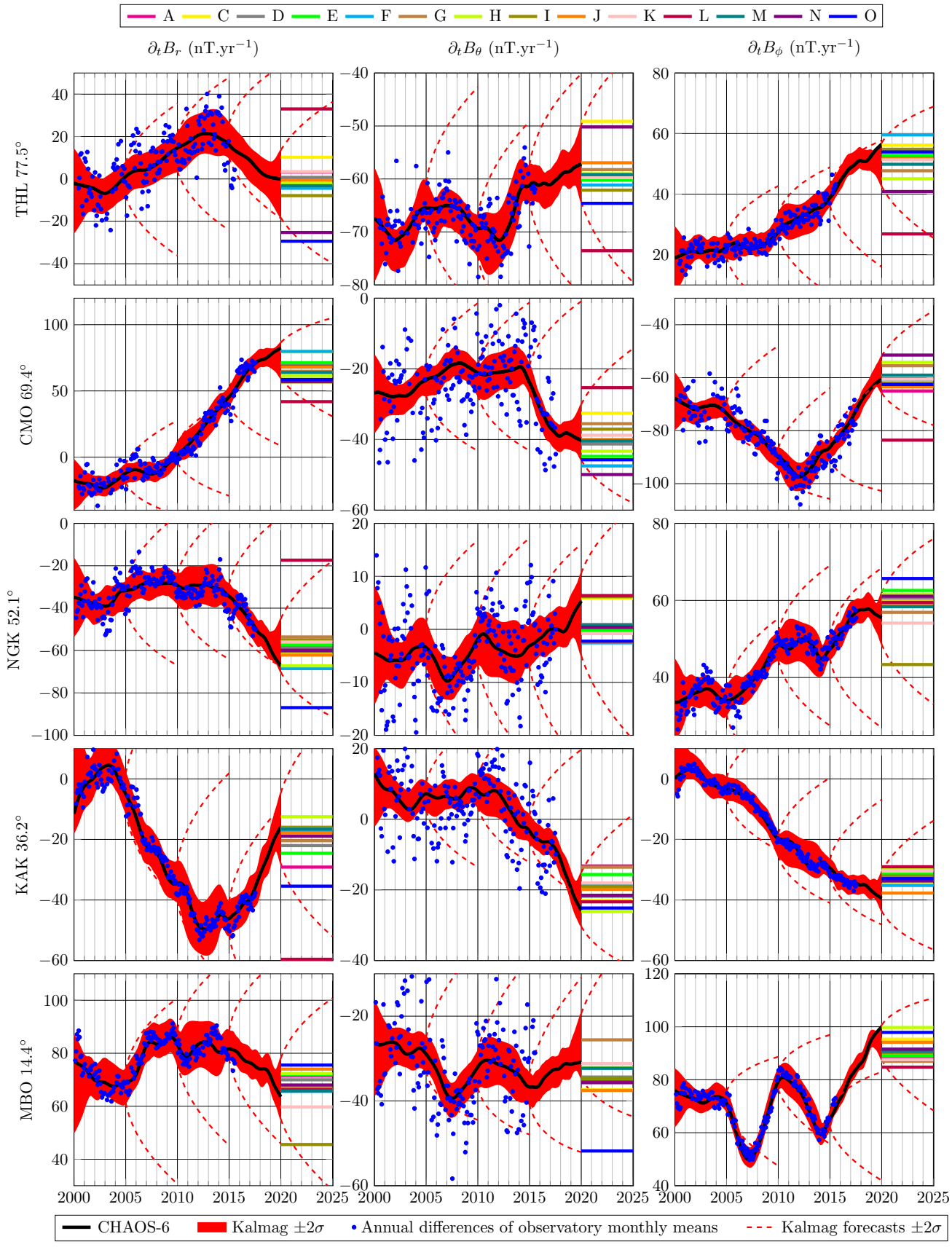

Figure 4: Time series of the secular variation at the level of different ground based observatories

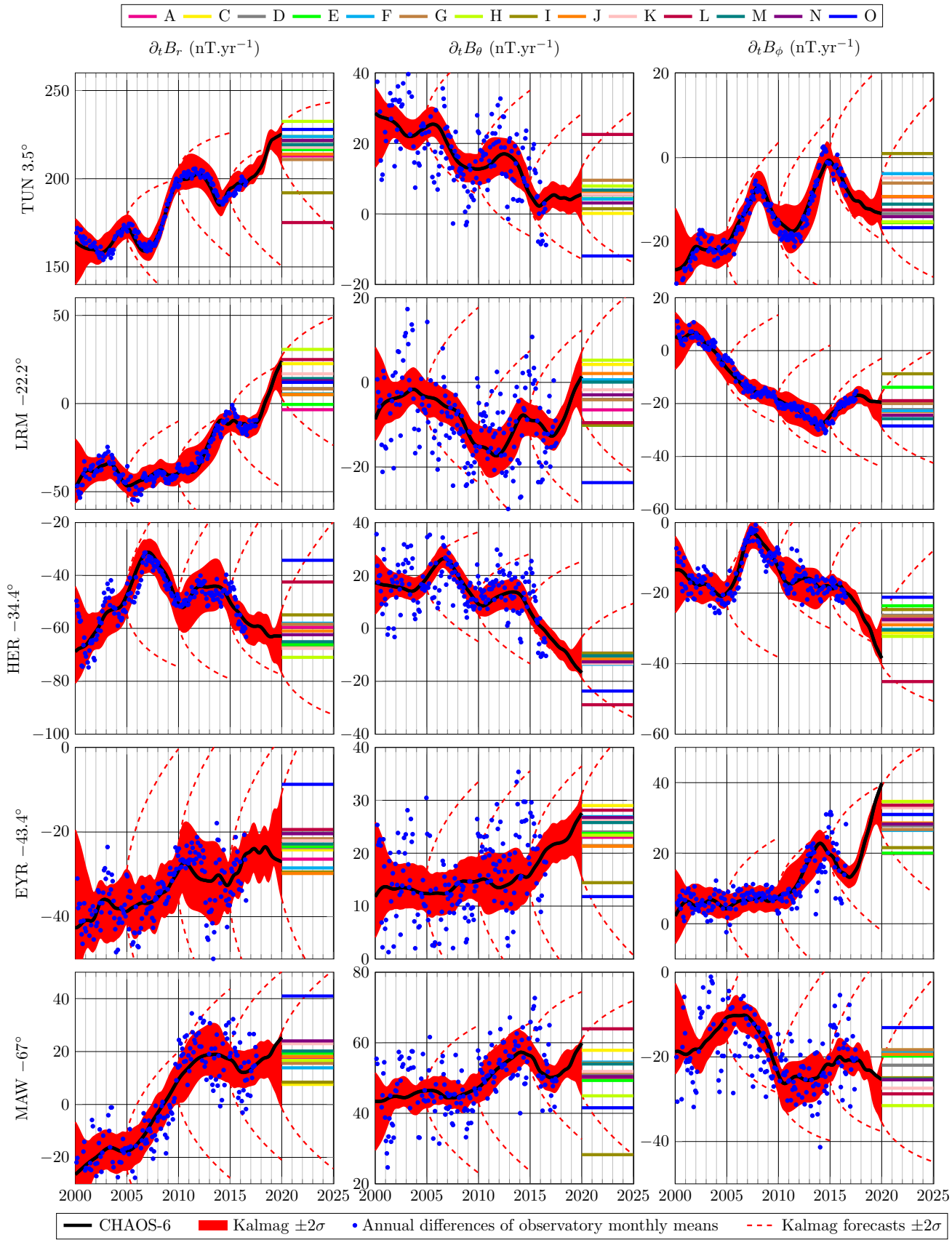

Figure 5: Time series of the secular variation at the level of different ground based observatories

3.2 Harmonic coefficients time series

We look at the predictions for the different candidate models in the spherical harmonics domain, for a selection of large scale coefficients – up to harmonic degree 3. Similarly to the evaluation at the observatories locations, we compare – for

each candidate – how well the SV predicted over $2020.0 - 2025.0$ falls within the $\pm 2\sigma$ area of the Kalmag model forecast. Figure 6 displays the SV candidate models for harmonic coefficients $\dot{g}_1^0$, $\dot{g}_1^1$, $\dot{g}_2^0$, $\dot{g}_2^1$, $\dot{g}_2^{-1}$, $\dot{g}_3^1$. The corresponding degrees and orders are given at the top of every panel. Times series of the CHAOS-6 model (in black), and the Kalmag model (in red) are represented as well as the prediction over $2020.0 - 2025.0$ (in lighter red). The Kalmag time series and prediction are displayed with a 2σ width. The candidate models are presented with the same color assignments as in figures 4 and 5, again indicated at the top of the figure.

Again, we see that most of the models predict a close variation for the $2020.0 - 2025.0$ period, with means of the secular variation over the 5 years well within the 95% confidence interval. However, for some harmonic coefficients, the predictions of three of the candidates differ from the mean solution.

The candidate **L** (purple) differs notably from the other models at most degrees and orders. Its predictions for the coefficients $\dot{g}_2^1$ and $\dot{g}_3^1$ fall entirely without the predicted 95% confidence interval.

The model **O** (blue) seems to be in agreement with the other models for most coefficients except the dipole coefficient $\dot{g}_1^0$, and – less so – the $\dot{g}_1^1$. The latter doesn't fall entirely out of the $\pm 2\sigma$ area, but is in clear disagreement with the other models. Only candidate model **I** (olive green) presents a similar difference with the other candidates, although it should be noted that some discrepancies were also raised with this model. The **O** model's coefficient $\dot{g}_1^{-1}$ (not represented) is also quite far from the bulk, but this coefficient presents more dispersion among the different models. This result suggests that the differences observed for this model in the spatial domain are mostly due to a discrepancy in the dipole, as it was confirmed by the analysis without dipole. We note that the absolute value of the $\dot{g}_1^0$ coefficient for the **O** model is close to that of the other models, but with an opposite sign.

4 Conclusion

For the Main field 2020, there are only four candidate models that show significant differences relative to other models, namely models **B** , **E** and **O** and to a lesser extent model **N** . If an averaging process is used to derive the IGRF-13, as in previous IGRF editions, we recommend to perform this average in the space domain and to significantly down-weight models that present large differences relative to the median model.

For the $2020 - 2025$ secular variation, three candidate models exhibit noticeable deviations from the others, the **O** , the **I** and the **L** models. The **O** candidate is the only one predicting a negative value for the first time derivative of the dipole component g_1^0. This is the only aspect of the model strongly contradicting the other candidates. The **L** model is clearly the one deferring the most from the others. Contrary to the **I** candidate, the **L** model is incompatible with our Kalmag 2.5 years forecast. We therefore suggest that the **L** secular variation should be considered with extreme care.

References

[Finlay et al., 2016] Finlay, C. C., Olsen, N., Kotsiaros, S., Gillet, N., and Tøffner-Clausen, L. (2016). Recent geomagnetic secular variation from Swarm and ground observatories as estimated in the CHAOS-6 geomagnetic field model. *Earth, Planets, and Space*, 68:112.

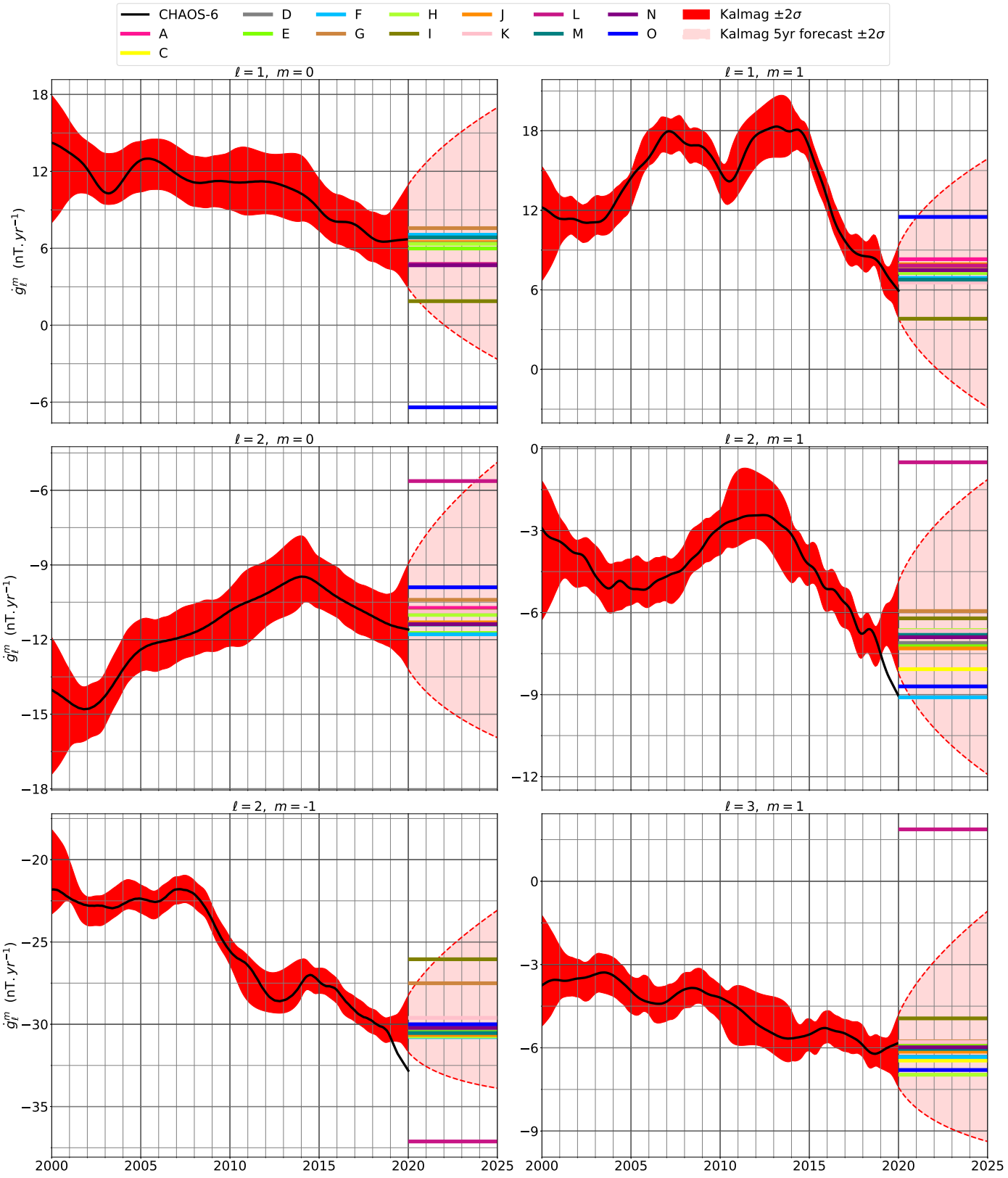

Figure 6: Time series for selected harmonic coefficients. From top left to bottom right : $\dot{g}_1^0$, $\dot{g}_1^1$, $\dot{g}_2^0$, $\dot{g}_2^1$, $\dot{g}_2^{-1}$, $\dot{g}_3^1$. Opaque red area : Kalmag mean time series with a $\pm 2\sigma$ width. Light red area : Kalmag forecast for $2020.0 - 2025.0$ with a $\pm 2\sigma$ width. Black line : Chaos-6 time series over $2000.0 - 2020.0$. The candidates are represented by horizontal lines, with a color code described at the top of the figure.